Atomic-resolution structures from fragmented protein crystals with the cryoEM method MicroED

M Jason de la Cruz[1], Johan Hattne[1], Dan Shi[1], Paul Seidler[2], Jose Rodriguez[2], Francis E Reyes[1], Michael R Sawaya[2], Duilio Cascio[2], Simon C Weiss[3], Sun Kyung Kim[3], Cynthia S Hinck[3], Andrew P Hinck[3], Guillermo Calero[3], David Eisenberg[2] & Tamir Gonen[1]

Traditionally, crystallographic analysis of macromolecules has depended on large, well-ordered crystals, which often require significant effort to obtain. Even sizable crystals sometimes suffer from pathologies that render them inappropriate for high-resolution structure determination. Here we show that fragmentation of large, imperfect crystals into microcrystals or nanocrystals can provide a simple path for high-resolution structure determination by the cryoEM method MicroED and potentially by serial femtosecond crystallography.

Large and perfect crystals are desirable for traditional structure determination because they yield a strong signal over background. In reality, crystals of biological material are rarely perfect. In the mosaic model, a real, imperfect crystal is composed of several small but well-ordered blocks[1]. These mosaic blocks have a finite size, are misaligned with respect to each other, and may be composed of unit cells with different dimensions[2]. Depending on the nature and degree of disorder between the mosaic blocks, an imperfect crystal may exhibit a plethora of pathologies, which may hamper subsequent data reduction, limit the resolution of the final model, and even prevent structure determination altogether (**Supplementary Figs. 1–9**).

Small crystals are usually not affected by such defects and therefore may yield superior data quality where diffraction is not limited by the number of diffracting unit cells in the crystal[3]. For these reasons, methods such as serial femtosecond crystallography (SFX)[4] at an X-ray free-electron laser (XFEL) and the electron cryomicroscopy (cryoEM) method microelectron diffraction (MicroED)[5] are actively being developed. These methods can yield structures to resolutions better than 1 Å from crystals that are significantly smaller than those which are required for standard crystallography, ~10,000× smaller in volume for XFEL and ~1,000,000× smaller for MicroED. In fact, in both these techniques large crystals can prove problematic. This is because large crystals can clog up the nozzle of liquid jet-based SFX sample delivery systems[6,7], while in MicroED the large electron-scattering cross-section implies that absorption extinguishes diffraction when the sample is too thick[8].

Here we show that sonication, vigorous pipetting, or vortexing can be used to break large imperfect crystals into small, single-crystal fragments that are suitable for data collection and atomic structure determination by MicroED (**Fig. 1**). Delicate samples may benefit from gentler fragmentation by vortexing, while harsher methods such as pipetting and sonication are required to break more robust crystals.

Fragmentation was tested on eight proteins with molecular weights ranging from 0.7 to 34.6 kDa and solvent contents between 30% and 60%: lysozyme, TGF-βm–TßRII, xylanase, thaumatin, trypsin, proteinase K, thermolysin, and a segment of the tau protein (**Fig. 2**, left column). Six of these proteins are standard samples that readily form crystals that are large—too big for MicroED and SFX experiments using liquid injectors—and without crystal growth optimization sometimes exhibit pathologies. Two of the samples (the TGF-βm–TßRII complex and tau peptide) represent challenging, new cases. As with the standard samples, we could obtain large and imperfect crystals for TGF-βm–TßRII complex and tau without growth optimization. These large crystals were broken apart by one of the three fragmentation approaches (see Online Methods) before preparation on cryoEM grids. Micrometer- or nanometer-sized crystal fragments appeared evenly distributed on the grid; and even when grids were densely populated, single-crystal data sets could be collected by using the selected area aperture.

In many cases, the untreated crystals were mosaic, yielded diffraction patterns with multiple lattices, or were otherwise unsuitable for standard crystallographic experiments (**Fig. 1** and **Supplementary Figs. 1–9**). In the case of the amyloid-forming peptide of tau, what appeared to be large crystals were in fact crystal bundles that produced low-resolution powder-like diffraction. These problems have traditionally been overcome by modifying the crystallization conditions to optimize crystal growth and quality—a process that can be tedious and labor intensive, particularly when crystal pathologies do not become apparent until data processing. Breaking of large crystals by physical means produced fragments that appeared crystallographically

[1]Howard Hughes Medical Institute, Janelia Research Campus, Ashburn, Virginia, USA. [2]Howard Hughes Medical Institute, UCLA-DOE Institute, Departments of Biological Chemistry, Chemistry & Biochemistry, and Molecular Biology Inst tute, UCLA, Los Angeles, California, USA. [3]Department of Structural Biology, University of Pittsburgh, Pittsburgh, Pennsylvania, USA. Correspondence should be addressed to T.G. (gonent@janelia.hhmi.org).

RECEIVED 2 AUGUST 2016; ACCEPTED 28 DECEMBER 2016; PUBLISHED ONLINE 13 FEBRUARY 2017; DOI:10.1038/NMETH.4178

homogeneous and yielded diffraction data at atomic resolution and void of the above artifacts (**Supplementary Table 1**). MicroED has already allowed rapid structure determination from several peptide fragments that could not be solved using microfocus synchrotron sources in spite of many months of crystal optimization (**Supplementary Figs. 2–4**). For each sample, data

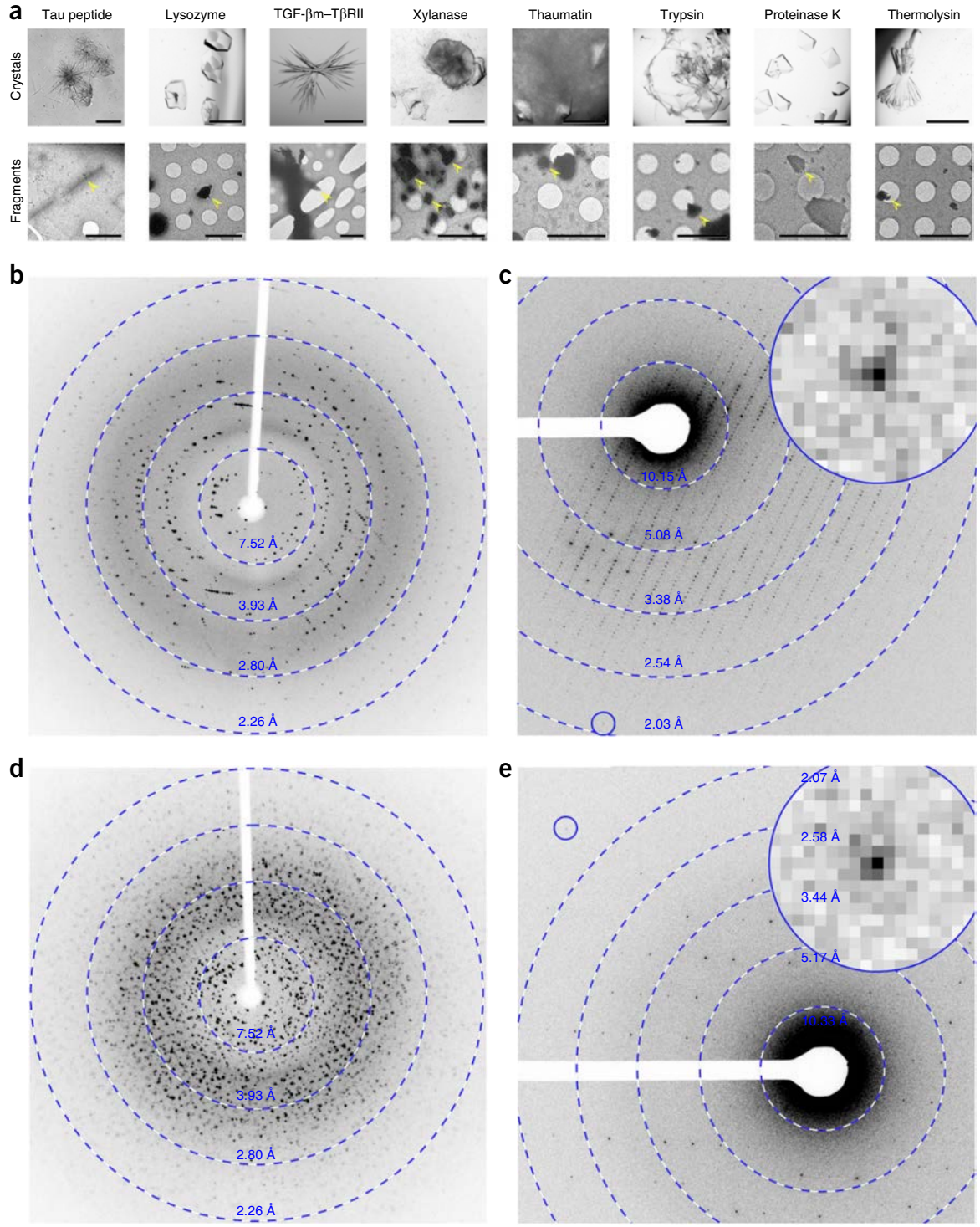

Figure 1 | Crystals before and after fragmentation and their X-ray and MicroED diffraction patterns. (**a**) Top row, light micrographs of imperfect crystals before fragmentation. Scale bars are 500 µm, except for tau peptide and TGF-βm–TßRII, where the scale bar is 50 µm. Bottom row, electron micrographs of fragmented crystals. Scale bars are 5 µm. (**b**) An example of X-ray diffraction from a thaumatin crystal exhibiting multiple lattices. (**c**) MicroED from a fragmented thaumatin crystal does not suffer from the same pathologies. (**d**) An example of X-ray diffraction from trypsin crystals yielding only powder-like diffraction. (**e**) MicroED analysis of fragmented trypsin crystals does not suffer from the same pathologies. The inset shows a close up of the spot indicated by the blue circle. X-ray diffraction patterns were collected on a CuKα home over a 0.37° rotation range; MicroED patterns were recorded as detailed in the Online Methods. Further examples are shown in **Supplementary Figures 1–9**.

were collected from two to ten crystal fragments, and data sets were merged for completeness and multiplicity (**Supplementary Table 1**). Although we have previously published two structures where a single nanocrystal was sufficient for structure determination[9,10], multicrystal merging is generally preferred. This is partly because the grid on which the crystals are mounted limits the accessible rotation range during data collection and partly because small, weakly scattering samples require a more intense beam to yield statistically accurate measurements of the Bragg reflections and may be irreversibly damaged before a complete data set can be obtained. Recording narrow wedges with fewer exposures for each crystal involves a trade-off between limiting the damage to the sample and maintaining sufficient beam intensity for the signal from high-resolution reflections to be accurately integrated. Because the resolutions obtained by MicroED are comparable to or better than those obtained by X-ray diffraction before sonication, it appears that fragmentation only broke apart the large crystals into small crystal domains and did not otherwise damage the lattice order.

The macromolecular structures in this study were phased using molecular replacement (MR) or by direct methods and refined using electron-scattering factors[11]. In all cases, the refined model fits the calculated density well (**Fig. 2**, middle column) with an overall real-space correlation coefficient ranging from 0.72 to 0.91 (RSCC; **Supplementary Table 1**). The resulting simulated-annealing (SA) composite omit maps (**Fig. 2**, right column) match their respective models very well, indicating that the data are indeed high quality and unbiased. Further, the SA omit maps for lysozyme reveal depressions or holes in the aromatic rings of amino acid side chains, while for proteinase K toroidal densities were observed even for proline residues at the 1.6-Å resolution cutoff. A well-coordinated calcium ion is clearly visible in the omit map for trypsin, as is one of the iodides in the xylanase structure. Individual atoms are visible in the density for the tau peptide, and several residues show positive $2mF_o–DF_c$ peaks for hydrogen atoms; for one residue, modeled hydrogens allowed us to unambiguously place the correct sidechain rotamer.

All structures were determined between 1.1–2.9-Å resolution. We note that the *R*-factors from model refinement are generally higher in MicroED than are typical values obtained in X-ray crystallography at similar resolutions. Others and we have made such observations in previously published studies[5,9,12]. We believe that the main reason for this is the lack of adequate electron-scattering factors in the crystallographic refinement software. X-rays are scattered by the electron cloud of an atom, while electrons are scattered by the atomic Coulomb potential, which arises from the nucleus as well as its surrounding electrons. Current electron-scattering-factor tables do not properly account for this difference, and this may contribute to the residual between observed and calculated structure factor amplitudes leading to higher than normal crystallographic and free *R*-factors. We note that the gap between R_{work} and R_{free} is small, indicating no concerns of overfitting (**Supplementary Fig. 10**).

MicroED is inherently well suited to studying crystal fragments. Electrons interact strongly with matter so that large crystals are not required to detect high-resolution Bragg reflections[8]. MicroED has been used to determine the structures of the enzymes lysozyme[5,9], proteinase K[13], catalase[10,12], and Ca^{2+}-ATPase[12]. It was also recently used to solve the 1.4-Å-resolution structure of

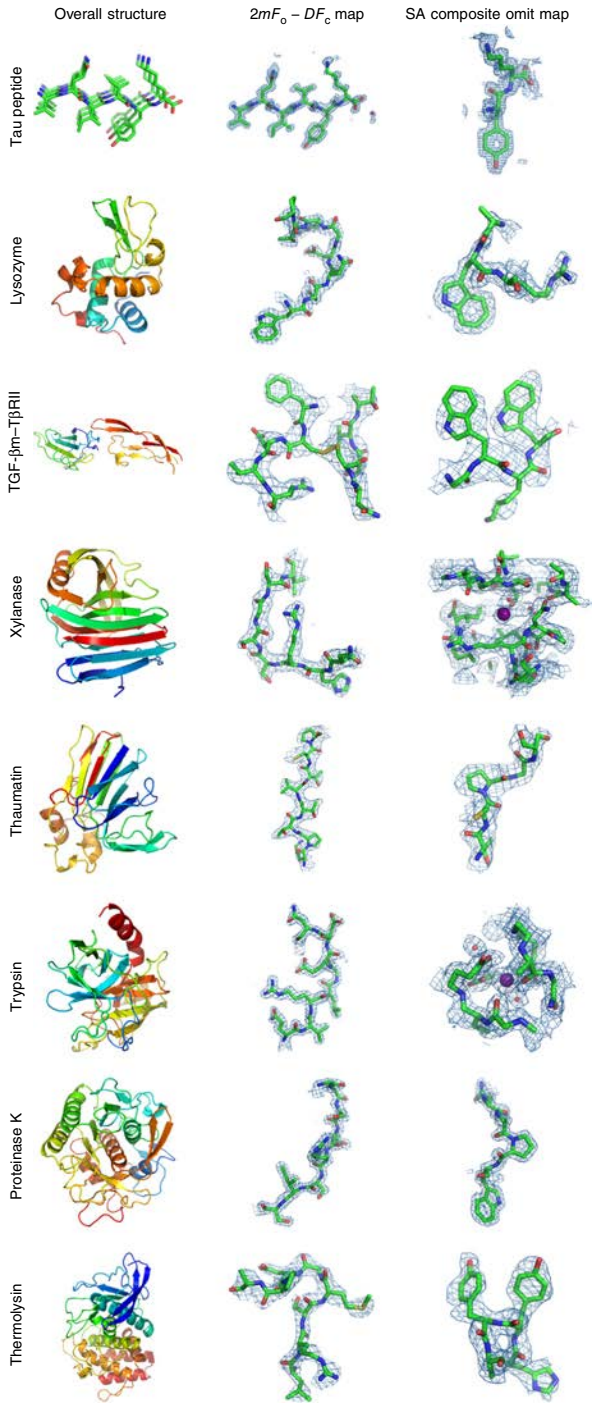

Figure 2 | Eight atomic-resolution structures determined by MicroED from crystal fragments. Left column, ribbon representations of the corresponding macromolecules. The tau peptide model indicates a β-sheet generated by crystal packing. Middle column, $2mF_o–DF_c$ charge density maps contoured at 1.5 σ above the mean, showing eight residues in loop regions of the respective structures, where *m* is the figure of merit and *D* is derived from coordinate error estimates. For TGF-βm–TßRII one of the disulfide bonds is shown. Right column, SA composite omit maps contoured at 1 σ above the mean, except for the maps from lysozyme and proteinase K, which are contoured at 1.5 σ above the mean. Depressions or holes can be observed in the density of side chains of aromatic residues for tau peptide and lysozyme, and for proline residues in the proteinase K structure. Iodide and calcium ions are visible in the omit maps for xylanase and trypsin, respectively. All figures were generated using PyMol[19].

the toxic nonamyloid-β component (NAC) core of α-synuclein, where diffraction data were collected from crystals smaller than the wavelength of visible light[14]. We previously demonstrated that crystals thinner than ~400 nm are suitable for MicroED and routinely yield atomic-resolution information. The highest resolution structures reported so far by using MicroED are from four prion protein fragments determined at 1-Å resolution solved by direct phasing methods[15].

Breaking large crystals into well-formed crystal fragments has a long history in crystallography; indeed, X-ray diffraction was discovered from broken-up pieces of a copper sulfate crystal[16]. Sonication[17] and vortexing[18] have previously been used to prepare crystals of suitable size for XFEL measurements by SFX. By breaking up one imperfect large crystal into thousands or even millions of smaller crystallites and recombining a well-diffracting subset during data processing, we have used MicroED to determine the structure of eight different proteins to high resolution. Fragmentation does not increase the effort required for sample screening, and future work on automation is expected to reduce the time for data collection irrespective of how the sample was prepared. As demonstrated by the breadth of size and packing of macromolecules whose crystals we investigated, we believe this approach will be broadly applicable whenever large crystals are available. Fragmentation widens the scope of diffraction methods such as MicroED and SFX to include samples that do not exclusively form tiny crystals but instead form large, imperfect crystals.

METHODS

Methods, including statements of data availability and any associated accession codes and references, are available in the online version of the paper.

Note: Any Supplementary Information and Source Data files are available in the online version of the paper.

ACKNOWLEDGMENTS

The Gonen laboratory is supported by funds from the Howard Hughes Medical Institute. The Eisenberg laboratory is supported by HHMI, NIH grant 1R01-AG029430 (D.E.), and DOE grant DE-FC02-02ER63421 (D.E.). The Calero laboratory is supported by NIH grants R01GM120292 and R01DK102495 (G.C.) and BioXFEL-STC1231306 (G.C.). The Hinck laboratory is supported by NIH grants R01-GM58670 and R01-CA172886 (A.P.H.).

AUTHOR CONTRIBUTIONS

D.S. and T.G. designed the experiment; M.J.d.l.C. and F.E.R. prepared lysozyme, xylanase, thaumatin, trypsin, proteinase K, and thermolysin samples; J.R. prepared tau peptide samples; S.C.W., S.K.K., C.S.H., A.P.H., and C.G. prepared TGF-βm–TßRII samples; M.J.d.l.C., D.S., J.R., and S.C.W. collected data; M.J.d.l.C., J.H., P.S., M.R.S., D.C., S.C.W., and G.C. analyzed data and refined and determined models; J.H., J.R., and M.R.S. prepared figures; M.J.d.l.C., J.H., and T.G. wrote the manuscript with contributions from all authors.

COMPETING FINANCIAL INTERESTS

The authors declare no competing financial interests.

1. Darwin, C.G. *Philisophical Magazine Series 6* **43**, 800–829 (1922).
2. Nave, C. *Acta Crystallogr. D Biol. Crystallogr.* **54**, 848–853 (1998).
3. Cusack, S. *et al. Nat. Struct. Biol.* **5** (Suppl.), 634–637 (1998).
4. Schlichting, I. *IUCrJ* **2**, 246–255 (2015).
5. Shi, D., Nannenga, B.L., Iadanza, M.G. & Gonen, T. *eLife* **2**, e01345 (2013).
6. Weierstall, U. *Phil. Trans. R. Soc. Lond. B* **369**, 20130337 (2014).
7. Sierra, R.G. *et al. Acta Crystallogr. D Biol. Crystallogr.* **68**, 1584–1587 (2012).
8. Henderson, R. *Q. Rev. Biophys.* **28**, 171–193 (1995).
9. Nannenga, B.L., Shi, D., Leslie, A.G.W. & Gonen, T. *Nat. Methods* **11**, 927–930 (2014).
10. Nannenga, B.L., Shi, D., Hattne, J., Reyes, F.E. & Gonen, T. *eLife* **3**, e03600 (2014).
11. Colliex, C. *et al.* in *International tables for crystallography*, Vol. C (eds. Prince, E. & Wellberry, T.R.) Ch. 4.3 (International Union of Crystallography, 2006).
12. Yonekura, K., Kato, K., Ogasawara, M., Tomita, M. & Toyoshima, C. *Proc. Natl. Acad. Sci. USA* **112**, 3368–3373 (2015).
13. Hattne, J., Shi, D., de la Cruz, M.J., Reyes, F.E. & Gonen, T. *J. Appl. Crystallogr.* **49**, 1029–1034 (2016).
14. Rodriguez, J.A. *et al. Nature* **525**, 486–490 (2015).
15. Sawaya, M.R. *et al. Proc. Natl. Acad. Sci. USA* **113**, 11232–11236 (2016).
16. Von Laue, M. in *Nobel Lectures Physics 1901–1921*, 347–355 (Elsevier, 1967).
17. Stevenson, H.P. *et al. Acta. Crystallogr. D Struct. Biol.* **72**, 603–615 (2016).
18. Bublitz, M. *et al. IUCrJ* **2**, 409–420 (2015).
19. The PyMOL Molecular Graphics System v. 1.8 (Schrödinger, LLC, 2015).

ONLINE METHODS

Protein crystallization. Large crystals (>500 µm along the longest edge) were grown via hanging-drop vapor diffusion at room temperature using previously established protocols. All enzymes were purchased from Sigma-Aldrich (St. Louis, Missourri) unless otherwise noted.

Tau peptide (VQIVYK) was dissolved in distilled water, and crystals were prepared by mixing tau peptide with arachidonic acid and meclocycline sulfosalicylate. Crystals formed with a 1:2 drop peptide to precipitant ratio from 65–70% ethylene glycol in Tris pH 8.5.

Lysozyme (*G. gallus*) crystals were prepared by equilibrating 50 mg/ml lysozyme in 50 mM sodium acetate over 1.7 M sodium chloride, 50 mM sodium acetate pH 4.7.

TGF-βm–TßRII was expressed and purified as described before (ref. 20 and unpublished data). Crystals were grown from 0.5 µl of protein (20 mg/ml), 0.25 µl mother liquor, and 0.2 µl seed stock in 100 mM HEPES–NaOH pH 7.5 and 45% MPD.

Xylanase from *T. reesei* (Hampton Research, Aliso Viejo, California) was dialyzed against 10 mM bicine pH 9.0, 1 mM magnesium sulfate, and 1 mM DTT; and it was combined with a precipitant solution containing 0.3 M sodium iodide, 1.2–1.3 M ammonium sulfate, and 100 mM bicine pH 9.0 (ref. 21).

Thaumatin (*T. daniellii*) crystals were grown from 2 µL of protein (25 mg/ml in water) and Hampton Research Index Reagent 26 (1.1 M ammonium tartate pH 7.0).

Trypsin (*B. taurus*) was dissolved (60 mg/ml) in 10 mg/ml benzamidine, 3 mM calcium chloride and equilibrated against 4% (w/v) PEG4000, 0.2 M lithium sulfate, 0.1 M MES pH 6.5, and 15% ethylene glycol.

Proteinase K (*E. album*) crystals were grown by combining 2 µL of protein solution (50 mg/ml) with 2 µL of precipitant solution (1.0–1.3 M ammonium sulfate, 0.1 M Tris pH 8.0)[13].

Thermolysin from *B. thermoproteolyticus* (Hampton Research, Aliso Viejo, California) crystals were prepared by equilibrating a 160 mg/ml solution of thermolysin (45% dimethyl sulfoxide, 50 mM Tris pH 7.5, and 2.5 M cesium chloride) over 0.5 ml of water[22].

Crystal fragmentation. Drops containing the crystals were placed in separate microfuge tubes and suspended in crystal mother liquor. A sonicating water bath with electronic control (Elmasonic P30H, Singen, Germany) was set at its lowest power (30% at 37 kHz) for gentle agitation of the crystals in the tube. With the tube sealed, its tip was briefly submerged in the activated water bath for 0.5 s. Alternatively, crystals were fragmented by vigorously pipetting a crystal suspension in mother liquor (trypsin and thaumatin) or vortexed with 0.5 mm disruption glass beads in a 1.5 ml reaction tube for 2 s (TGF-βm–TßRII). A detailed protocol for crystal fragmentation is available as a **Supplementary Protocol** and is published online[23].

MicroED data collection. The solution containing fragmented crystals was then applied to transmission electron microscope (TEM) grids with carbon film support, and it was plunge frozen in liquid ethane. Frozen grids were mounted in a Gatan Model 626 cryospecimen holder and examined using an FEI Tecnai F20 field-emission TEM operated at an accelerating voltage of 200 kV, which corresponds to a de Broglie wavelength of 0.025 Å, and the grids were screened for crystals in over-focused diffraction mode. Where a single still shot revealed strong diffraction, data were collected as continuous rotation-tilt series[9]. Individual frames were recorded on a TVIPS TemCam-F416 as 4 s exposures while the stage was rotating at 0.09°/s, except for tau peptide, which was rotated at 0.29°/s during 2 s exposures. For the macromolecular samples, the absolute tilt angle was generally <35° (<65° for tau peptide). Data sets collected from each crystal spanned between 30° and 135°, corresponding to a total dose no greater than 1.2–5.5 e–/Å^2 at the given rotation rate. The selected area aperture of the TEM was used to limit the area from which data were collected, making it possible to select a single crystal fragment. The virtual detector distance varied between 0.73 mm and 3.6 m for the different data sets, corresponding to a maximum resolution between 0.95 Å and 2.0 Å in the detector corners at an acceleration voltage of 200 kV. The movie frames recorded in rolling-shutter mode on the TVIPS TemCam-F416 CMOS camera were converted to SMV format, while preserving as much as possible of the metadata necessary for subsequent processing[24]. Detailed protocols for data collection were recently published[25].

Structure determination. Sweeps were corrected to account for negative pixel values[13], then they were indexed and integrated in MOSFLM[26] using its graphical interface iMOSFLM[27] or in XDS[28]. To further probe the scattering power of the crystallites, diffraction patterns were initially processed without imposing any resolution cutoffs other than those entailed by the geometry of the experiment. Except for the tau peptide and TGF-βm–TßRII, the high-resolution limits due to factors other than the area of the detector were instead determined case by case to give stable processing during refinement of the atomic model. Multicrystal scaling and merging were performed in AIMLESS[29]. Structures were phased by molecular replacement using MOLREP[30] from the PDB entries 3j6k, 1ktz, 2dfb, 4ek0, 2ptn, 5i9s, and 2tli for lysozyme, TGF-βm–TßRII, xylanase, thaumatin, trypsin, proteinase K, and thermolysin, respectively, or by direct methods using SHELXT[31]. A free *R* set comprising approximately 5% of the unique reflections was copied from the deposited data for each search model. The deposited data for the xylanase and trypsin models do not define a free set; instead, a new set was chosen using freerflag[32].

Maximum likelihood structure refinement was carried out in phenix.refine[33] using electron-scattering factors[11]. Explicit water molecules were automatically modeled by phenix.refine and subsequently manually curated in Coot[34]. SA composite omit maps were computed from the refined models using CNS[35] with electron-scattering factors[36]. For these calculations, charged species were manually removed from the phasing models because they are not included in CNS's electron-scattering library. The SA protocol was defined to exclude ~5% of the structure at a starting temperature of 2,500 K. Protocols for data analysis in MicroED were recently published[25].

Statistics. The number of values used to calculate the statistics in **Supplementary Table 1** are given as "# total reflections" and "# unique reflections." No other statistical tests are used in the manuscript.

Data availability statement. Atomic coordinates and structure factors were deposited to the Protein Data Bank (PDB; 5k7n,

5k7o, 5ty4, 5k7p, 5k7q, 5k7r, 5k7s, and 5k7t) and the Electron Microscopy Data Bank (EMDB; 8216, 8217, 8472, 8218, 8219, 8220, 8221, and 8222), and the raw data were uploaded to the Structural Biology Data Grid[37] (10.15785/SBGRID/284, 10.15785/SBGRID/285, 10.15785/SBGRID/368, 10.15785/SBGRID/286, 10.15785/SBGRID/287, 10.15785/SBGRID/288, 10.15785/SBGRID/289, and 10.15785/SBGRID/290).

20. Zúñiga, J.E. *et al. J. Mol. Biol.* **354**, 1052–1068 (2005).
21. Watanabe, N., Akiba, T., Kanai, R. & Harata, K. *Acta Crystallogr. D Biol. Crystallogr.* **62**, 784–792 (2006).
22. English, A.C., Done, S.H., Caves, L.S.D., Groom, C.R. & Hubbard, R.E. *Proteins* **37**, 628–640 (1999).
23. de la Cruz, M.J. *et al.* Micro- and nanocrystal preparation for MicroED and XFEL serial crystallography by fragmentation of imperfect crystals. *Protocol Exchange* http://dx.doi.org/10.1038/protex.2017.010 (2017).
24. Hattne, J. *et al. Acta Crystallogr. A Found. Adv.* **71**, 353–360 (2015).
25. Shi, D. *et al. Nat. Protoc.* **11**, 895–904 (2016).
26. Leslie, A.G.W. & Powell, H.R. (eds.) *Evolving Methods for Macromolecular Crystallography* (Springer, 2007).
27. Battye, T.G.G., Kontogiannis, L., Johnson, O., Powell, H.R. & Leslie, A.G.W. *Acta Crystallogr. D Biol. Crystallogr.* **67**, 271–281 (2011).
28. Kabsch, W. *Acta Crystallogr. D Biol. Crystallogr.* **66**, 125–132 (2010).
29. Evans, P.R. & Murshudov, G.N. *Acta Crystallogr. D Biol. Crystallogr.* **69**, 1204–1214 (2013).
30. Vagin, A. & Teplyakov, A. *J. Appl. Crystallogr.* **30**, 1022–1025 (1997).
31. Sheldrick, G.M. *Acta Crystallogr. A Found. Adv.* **71**, 3–8 (2015).
32. Winn, M.D. *et al. Acta Crystallogr. D Biol. Crystallogr.* **67**, 235–242 (2011).
33. Afonine, P.V. *et al. Acta Crystallogr. D Biol. Crystallogr.* **68**, 352–367 (2012).
34. Emsley, P., Lohkamp, B., Scott, W.G. & Cowtan, K. *Acta Crystallogr. D Biol. Crystallogr.* **66**, 486–501 (2010).
35. Brunger, A.T. *Nat. Protoc.* **2**, 2728–2733 (2007).
36. Gonen, T. *et al. Nature* **438**, 633–638 (2005).
37. Meyer, P.A. *et al. Nat. Commun.* **7**, 10882 (2016).

doi:10.1038/nmeth.4178

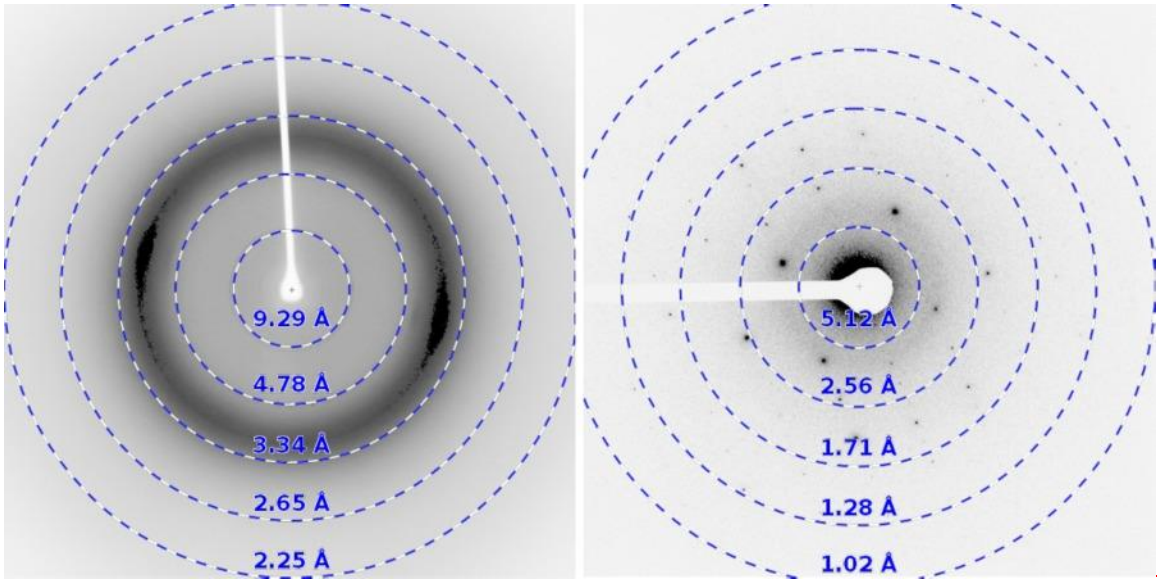

Supplementary Figure 1

X-ray and corresponding MicroED diffraction pattern from protein tau.

(Left) When extracted from hanging drops, a cluster of microneedle crystals of the amyloid-forming protein tau diffracts as powder to no better than 4.2 Å using a rotating anode X-ray source. Physically breaking these needle clusters and selecting individual sub-micron thick crystal fragments yields diffraction to atomic resolution by MicroED (right) and a structure solvable by direct methods. The X-ray diffraction pattern was collected over a 6° oscillation range; the MicroED pattern spans a 0.6° wedge. See main text for data collection details.

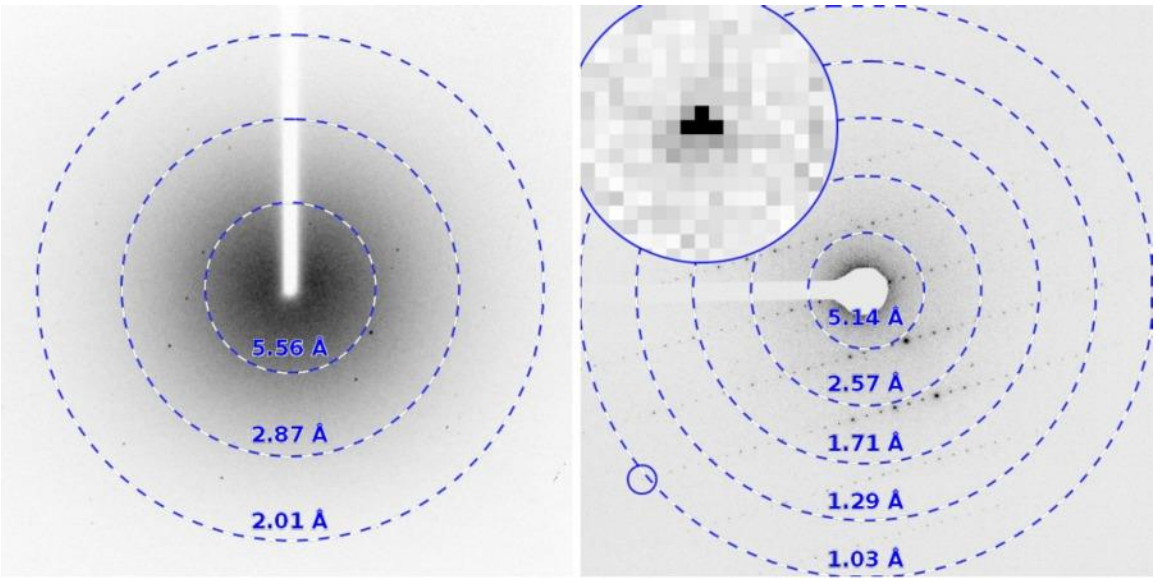

Supplementary Figure 2

X-ray and corresponding MicroED diffraction pattern from Zn^{2+}-NNQQNY.

The structure has previously been solved by X-ray diffraction, albeit at lower resolution [Nelson *et al.* (2005) Nature **435**, 773–778]. It was readily redetermined by direct methods from the MicroED data [Sawaya *et al.* (2016) Proc Natl Acad Sci **113**, 11232–11236]. For the MicroED pattern the inset shows a close-up of the spot indicated by the blue circle.

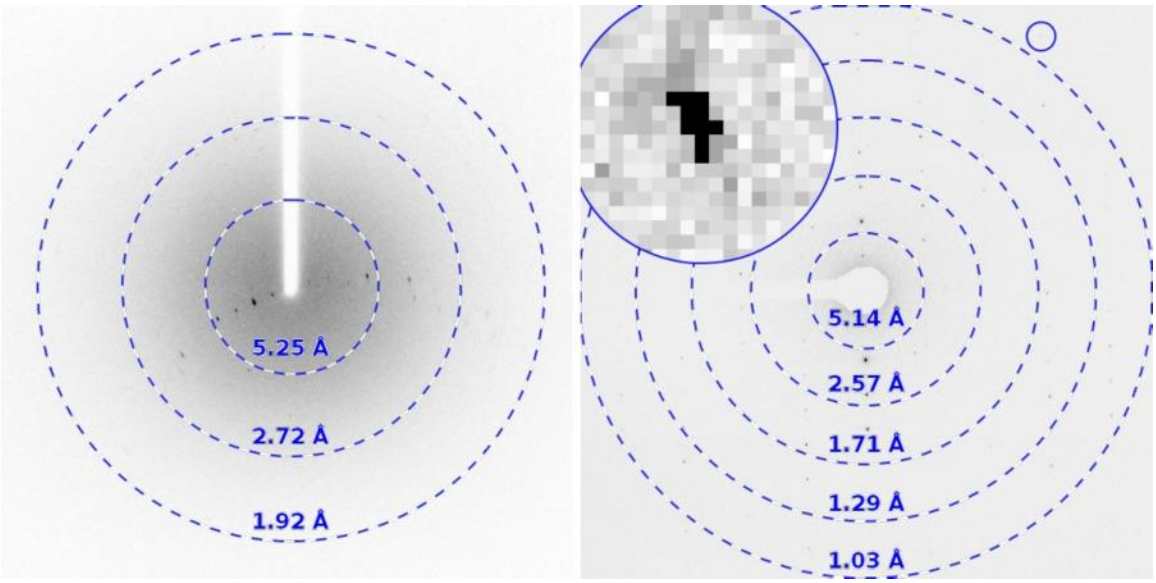

Supplementary Figure 3

X-ray and corresponding MicroED diffraction pattern from Cd^{2+}-NNQQNY.

This structure was not previously solved by X-ray diffraction, but was readily determined by direct methods from the MicroED data [Sawaya *et al.* (2016) Proc Natl Acad Sci **113**, 11232–11236]. For the MicroED pattern the inset shows a close-up of the spot indicated by the blue circle.

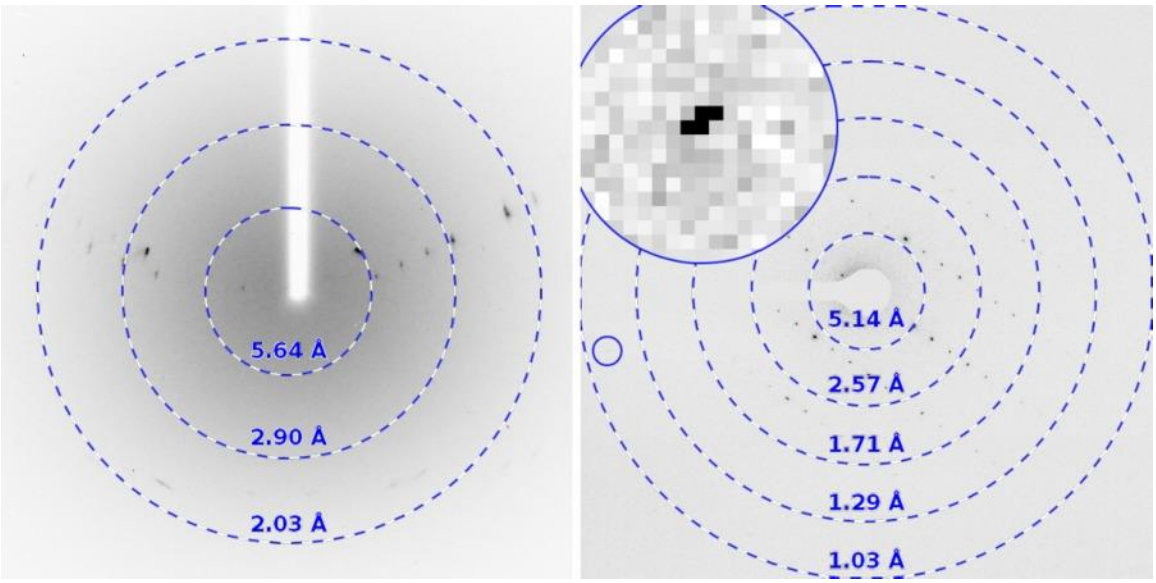

Supplementary Figure 4

X-ray and corresponding MicroED diffraction pattern from GNNQQNY.

The structure has previously been solved by X-ray diffraction, albeit at lower resolution [Nelson *et al.* (2005) Nature **435**, 773–778]. It was readily redetermined by direct methods from the MicroED data [Sawaya *et al.* (2016) Proc Natl Acad Sci **113**, 11232–11236]. For the MicroED pattern the inset shows a close-up of the spot indicated by the blue circle.

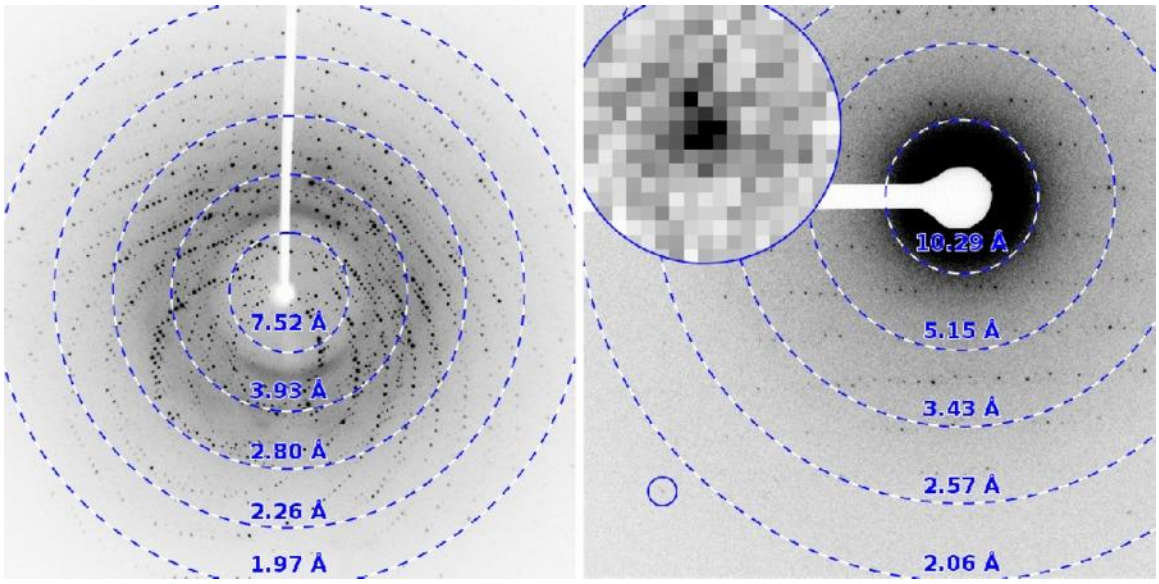

Supplementary Figure 5

X-ray and corresponding MicroED diffraction pattern from lysozyme.

The X-ray diffraction pattern displays multiple lattices. No optimization of crystal growth was done; instead crystals were sonicated and probed by MicroED. The obtained resolution was as good as what was obtained from the parent crystal. For the MicroED pattern the inset shows a close-up of the spot indicated by the blue circle.

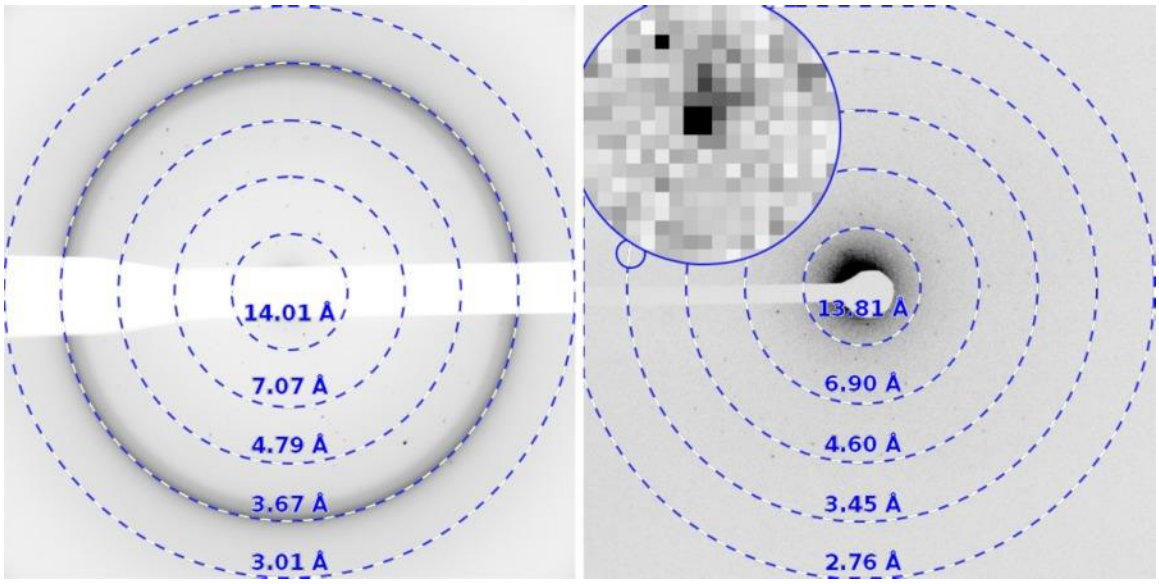

Supplementary Figure 6

X-ray and corresponding MicroED diffraction pattern from TGF-βm–TβRII.

The X-ray diffraction pattern was collected at an X-ray free-electron laser, but the crystals diffracted better under MicroED. No optimization of crystal growth was done; instead crystals were vortexed with glass beads and then probed by MicroED. For the MicroED pattern the inset shows a close-up of the spot indicated by the blue circle.

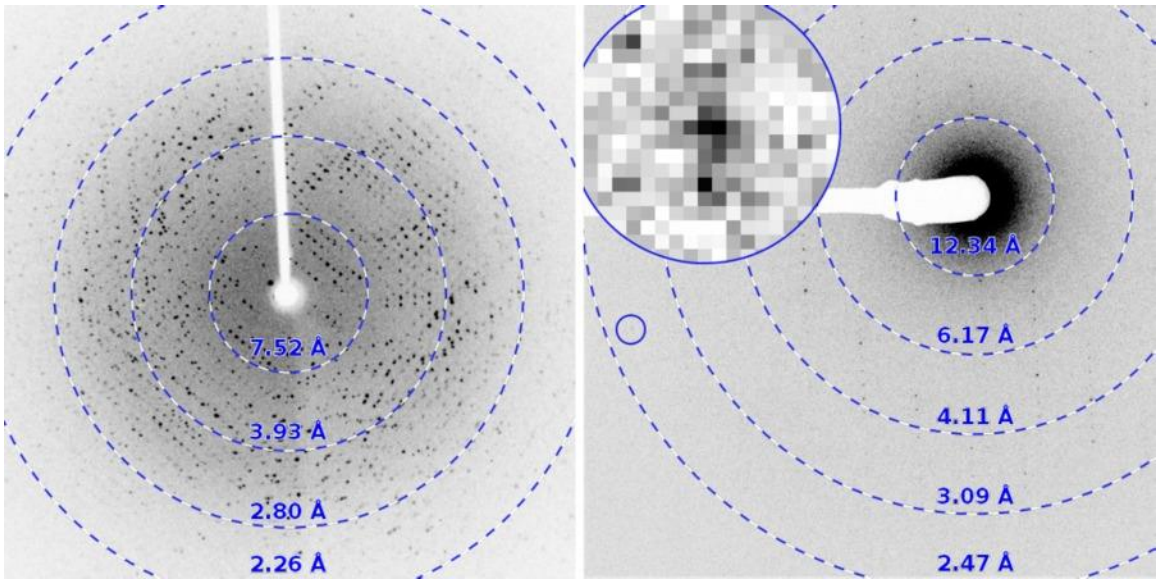

Supplementary Figure 7

X-ray and corresponding MicroED diffraction pattern from xylanase.

The X-ray diffraction pattern displays several multiple lattices. No optimization of crystal growth was done; instead crystals were sonicated and probed by MicroED. The obtained resolution was as good as what was obtained from the parent crystal. For the MicroED pattern the inset shows a close-up of the spot indicated by the blue circle.

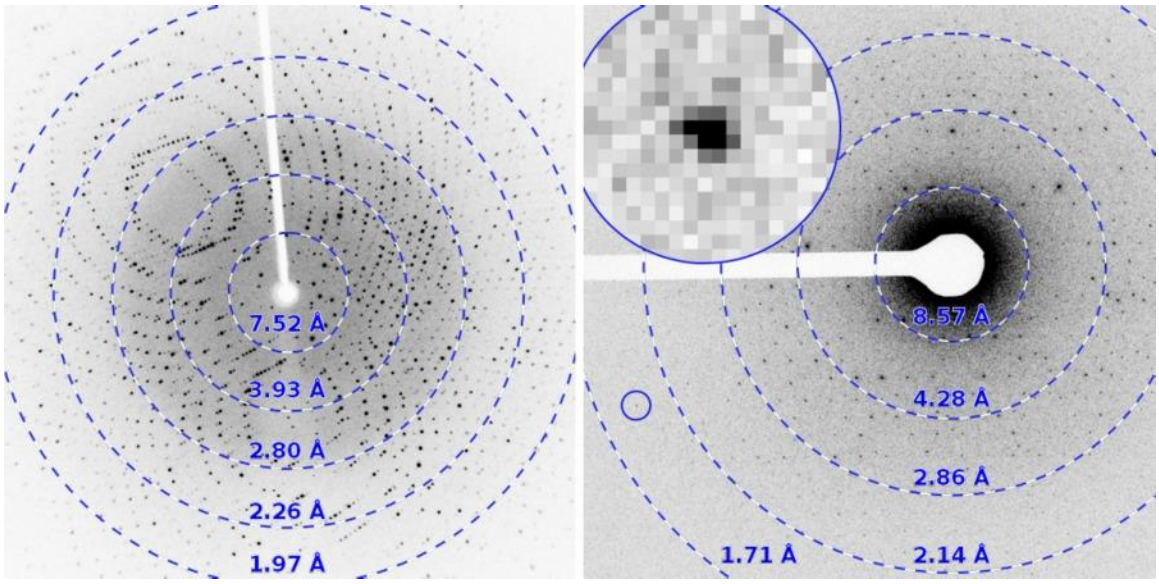

Supplementary Figure 8

X-ray and corresponding MicroED diffraction pattern from proteinase K.

The X-ray diffraction pattern displays multiple lattices. No optimization of crystal growth was done; instead crystals were sonicated and probed by MicroED. The obtained resolution was better than what was obtained from the parent crystal. For the MicroED pattern the inset shows a close-up of the spot indicated by the blue circle.

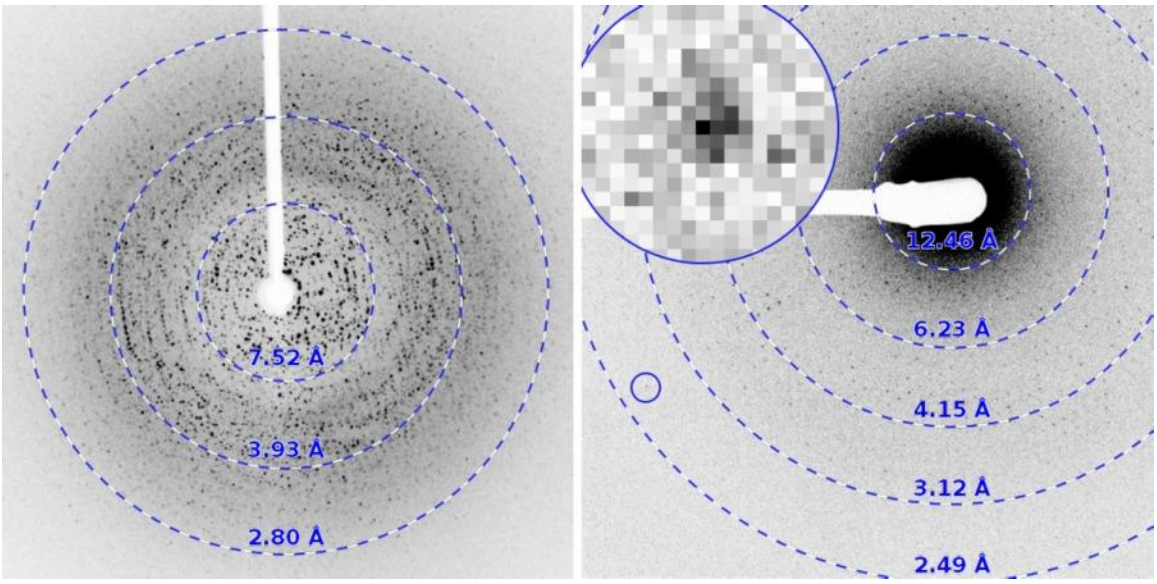

Supplementary Figure 9

X-ray and corresponding diffraction pattern from thermolysin.

The X-ray diffraction pattern is powder-like. No optimization of crystal growth was done; instead crystals were sonicated and probed by MicroED. The obtained resolution was better than what was obtained from the parent crystal. For the MicroED pattern the inset shows a close-up of the spot indicated by the blue circle.

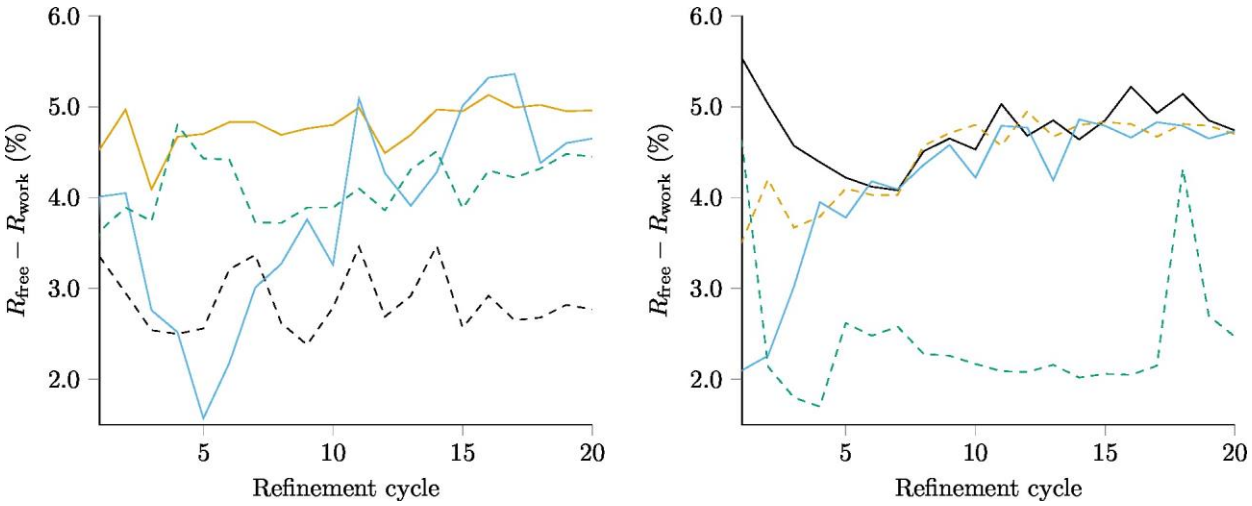

Supplementary Figure 10

R_{free} – R_{work} as a function of refinement cycle.

The *R*-factor gap is always less than 6% and the variation is generally within ±1% after the first few cycles. The variation is greater for TGF-βm–TβRII, thaumatin, and thermolysin, which are the lowest-resolution structures in this study. (Left) tau peptide (dashed black curve), lysozyme (solid orange curve), TGF-βm–TβRII (solid blue curve), and xylanase (dashed green curve). (Right) thaumatin (solid black curve), trypsin (dashed orange curve), proteinase K (solid blue curve), and thermolysin (dashed green curve). All refinements were performed using *phenix.refine* [Afonine *et al.* (2012) Acta Crystallogr D Biol Crystallogr **68**, 352–367].

Sample (PDB id; EMDB id)	Tau peptide (5k7n; EMD-8216)	Lysozyme (5k7o; EMD-8217)	TGF-βm:TβRII (5ty4; EMD-8472)	Xylanase (5k7p; EMD-8218)	Thaumatin (5k7q; EMD-8219)	Trypsin (5k7r; EMD-8220)	Proteinase K (5k7s; EMD-8221)	Thermolysin (5k7t; EMD-8222)
	Data collection							
Resolution (Å)	14.70–1.10	30.58–1.50	26.64–2.90	25.55–1.90	27.73–2.11	27.63–1.50	20.75–1.30	30.14–1.60
# crystals	2	7	3	4	3	10	6	4
<$T_{exposure}$> (s)	159.9	127.7	140.8	172.7	179.7	155.8	122.2	187.6
Molecular weight (kDa)	0.7	14.4	19.1	21.0	22.2	23.4	28.9	34.6
	Data processing							
Resolution[1] (Å)	14.70–1.10 (1.23–1.10)	30.58–1.80 (1.84–1.80)	26.64–2.90 (3.07–2.90)	25.55–2.30 (2.38–2.30)	27.73–2.51 (2.61–2.51)	27.63–1.70 (1.73–1.70)	20.75–1.60 (1.63–1.60)	30.14–2.50 (2.61–2.50)
Space group	*C*121	$P4_32_12$	$P2_12_12_1$	$P2_12_12_1$	$P4_12_12$	$P2_12_12_1$	$P4_32_12$	$P6_122$
Unit cell								
a, b, c (Å)	29.42, 4.99, 37.17	76.23, 76.23, 37.14	41.53, 71.33, 79.51	48.16, 59.75, 69.81	58.12, 58.12, 150.31	53.18, 56.43, 64.67	67.06, 67.06, 100.71	92.07, 92.07, 128.50
α, β, γ (°)	90, 111.55, 90	90, 90, 90	90, 90, 90	90, 90, 90	90, 90, 90	90, 90, 90	90, 90, 90	90, 90, 120
# total reflections[1]	6,185 (463)	88,734 (2,330)	14,911 (2,371)	32,523 (1,675)	39,272 (3.353)	137,532 (1,999)	246,199 (7,172)	137,511 (13,673)
# unique reflections[1]	3,319 (255)	10,372 (567)	3,884 (614)	7,774 (578)	8,868 (920)	19,843 (709)	29,968 (1,308)	11,203 (1,138)
$CC_{1/2}$[1]	0.987 (0.639)	0.901 (-0.013)	0.951 (0.255)	0.918 (0.052)	0.848 (0.071)	0.722 (0.071)	0.912 (0.051)	0.847 (0.201)
$\langle I/\sigma_I \rangle$[1]	2.4 (1.1)	3.7 (0.8)	3.3 (0.8)	3.5 (1.0)	3.5 (1.8)	2.6 (0.3)	3.4 (0.9)	5.6 (3.8)
Completeness[1]	83.0 (79.4)	97.6 (93.2)	71.9 (71.3)	85.4 (66.1)	94.2 (90.0)	90.1 (61.2)	96.8 (86.8)	97.1 (90.3)
Multiplicity[1]	1.9 (1.8)	8.6 (4.1)	3.8 (3.9)	4.2 (2.9)	4.4 (3.6)	6.9 (2.8)	8.2 (5.5)	12.3 (12.0)
	Refinement							
Resolution[1] (Å)	14.70–1.10 (1.12–1.10)	30.59–1.80 (2.06–1.80)	26.64–2.90 (3.65–2.90)	25.55–2.30 (2.63–2.30)	27.73–2.50 (2.86–2.50)	25.86–1.70 (1.79–1.70)	20.75–1.60 (1.64–1.60)	30.14–2.50 (2.75–2.50)
R_{work}[1] (%)	20.97 (21.04)	23.95 (32.33)	29.19 (36.11)	22.95 (35.40)	25.13 (34.08)	24.79 (38.72)	22.35 (36.33)	28.99 (34.78)
R_{free}[1,2] (%)	22.28 (22.43)	28.42 (37.94)	32.80 (36.87)	26.70 (38.95)	29.45 (38.98)	28.11 (42.37)	25.46 (42.25)	30.96 (36.64)
RSCC	0.84	0.89	0.72	0.85	0.86	0.89	0.91	0.86
# residues	6	129	166	190	207	223	279	316
# protein atoms	53	1,001	1,327	1,481	1,551	1,629	2,029	2,432
# water molecules	2	87	0	23	18	195	221	21
# ligand atoms	0	3	0	2	0	2	2	13
<ADP> (Å^2)								
Protein	12.4	13.4	47.8	25.5	20.3	13.9	8.1	4.9
Water	17.3	14.3		19.4	13.3	14.9	13.4	4.2
Ligand		16.7		66.5		19.6	18.9	7.5
R.m.s.d. bonds (Å)	0.012	0.004	0.012	0.002	0.002	0.005	0.004	0.003
R.ms.d. angles (°)	0.770	0.609	1.573	0.496	0.462	0.739	0.663	0.509
Ramachandran (outliers, favored) (%)	0.0, 100	0.0, 97.6	2.5, 89.9	0.0, 96.3	0.0, 95.1	0.0, 96.4	0.4, 96.8	0.0, 94.9

Supplementary Table 1

Data processing and model refinement statistics for the reported crystal structures.

Data sets were collected and processed as described in the online methods section. The dose rate did not exceed 0.01 $e^-/Å^2/s$ and the mean per-crystal exposure time is given as $\langle T_{exposure} \rangle$ for each sample. Except for tau peptide and TGF-βm:TβRII, reflections were initially integrated to the corners of the detector; the final resolution cutoff was determined based on $CC_{1/2}$ and the stability of the refinement procedure.

[1] Numbers in parentheses reflect the highest resolution shell for either data collection or refinement.

[2] In all cases the test set comprises approximately 5% of the unique reflections, where possible chosen to match that of the deposited data for the MR search model.